Supplementary Information

3D-Encapsulated Iridium-Complexed Nanophosphors for Highly Efficient Host-Free Organic Light-Emitting Diodes

Fuquan Han,[a] Xiaolin Zhang,[b] Jing Zhang,[a] Ying Wei,[ac] Xinwen Zhang,[b] Wei Huang[bc] and Hui Xu*[ac]*

[a] Key Laboratory of Functional Inorganic Material Chemistry, Ministry of Education & School of Chemistry and Material Science, Heilongjiang University, 74 Xuefu Road, Harbin 150080 (P. R. China)

[b] Key Laboratory for Organic Electronics and Information Displays (KLOEID), Institute of Advanced Materials (IAM), Nanjing University of Posts and Telecommunications, 9 Wenyuan Road, Nanjing 210023 (P. R. China)

[c] Key Laboratory of Flexible Electronics (KLOFE) & Institute of Advanced Materials (IAM), Jiangsu National Synergetic Innovation Center for Advanced Materials (SICAM), Nanjing Tech University, 30 South PuZhu Road, Nanjing 211800 (P. R. China)

Content

Experimental section

Materials and Instruments

All the reagents and solvents used for the synthesis of the compounds were purchased from Aldrich and Acros companies and used without further purification.

1H NMR spectra were recorded using a Varian Mercury plus 400NB spectrometer relative to tetramethylsilane (TMS) as internal standard. Molecular masses were determined by a FINNIGAN LCQ Electro-Spraying Ionization-Mass Spectrometry (ESI-MS), or a MALDI-TOF-MS. Elemental analyses were performed on a Vario EL III elemental analyzer. Absorption and photoluminescence (PL) emission spectra of the target compound were measured using a SHIMADZU UV-3150 spectrophotometer and a SHIMADZU RF-5301PC spectrophotometer, respectively. The neat and doped thin films of **Ir(*xy*NTCzPBI)$_3$** for analysis were prepared through vacuum evaporation on glass substrates under the same condition of device fabrication. The morphological characteristics of these films were measured with an atom force microscope (AFM) Agilent 5100 under the tapping mode. Thermogravimetric analysis (TGA) and differential scanning calorimetry (DSC) were performed on Shimadzu DSC-60A and DTG-60A thermal analyzers under nitrogen atmosphere at a heating rate of 10 °C min^{-1}. Cyclic voltammetric (CV) studies were conducted using an Eco Chemie B. V. AUTOLAB potentiostat in a typical three-electrode cell with a platinum sheet working electrode, a platinum wire counter electrode, and a silver/silver nitrate (Ag/Ag$^+$) reference electrode. All electrochemical experiments were carried out under a nitrogen atmosphere at room temperature in dichloromethane. Phosphorescence spectra were measured in dichloromethane using an Edinburgh FPLS 920 fluorescence spectrophotometer at 77 K cooling by liquid nitrogen. The time decay spectra was measured using Time-Correlated Single Photon Counting (TCSPC) method with a microsecond pulsed Xenon light source for 1 μs-10 s lifetime measurement, the synchronization photomultiplier for signal collection and

the Multi-Channel Scaling Mode of the PCS900 fast counter PC plug-in card for data processing.

General procedure of imidazole-cyclization reaction: In Ar, a mixture of benzene-1,2-diamine (2.7 g, 25 mmol), dihydroxybenzaldehyde (3.45 g, 25 mmol), $Na_2S_2O_5$ (4.75 g, 25 mmol) and dimethyl formamide (DMF, 100 mL) was heated to 90 ^oC and stirred for 24h. After cooling to room temperature, the mixture was poured into water. The precipitate was collected by filtration and purified by recrystallization from ethanol solutions.

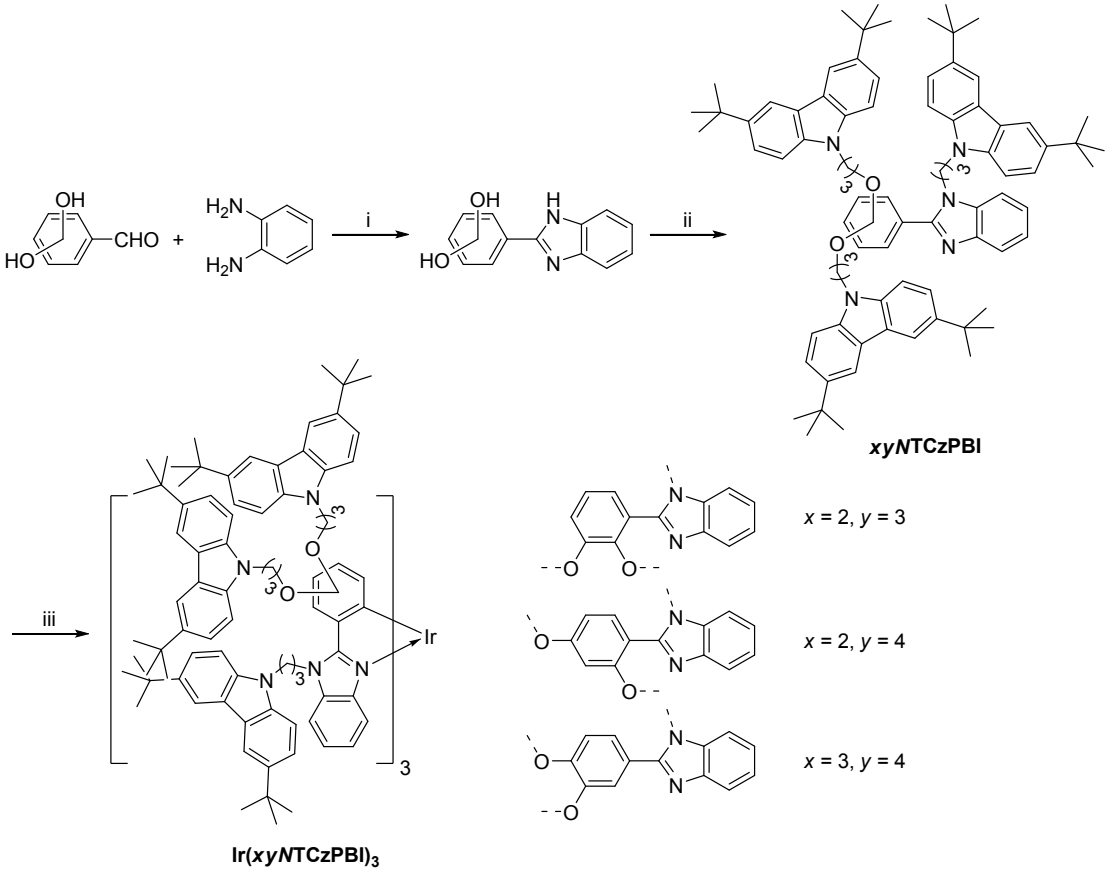

Scheme S1. Synthetic procedure of **Ir(*xy*NTCzPBI)$_3$**: i. $Na_2S_2O_5$, DMF, 90 ^oC, 24 h; ii. TBAB, KOH, 3,6-di-tert-butyl-*N*-(3-chloropropyl)-carbazole, THF, 80°C, 24 h; iii. .

3-(1H-benzo[d]imidazol-2-yl)benzene-1,2-diol: white powder with the yield of 72%. ^1H NMR (TMS, DMSO-d6, 400 MHz): δ = 13.183 (s, 2H), 9.209 (s, 1H), 7.700 (s, 1H), 7.611 (s, 1H), 7.483 (d, J = 7.6 Hz, 1H), 7.274 (d, J = 3.6 Hz, 2H), 6.892 (d, J = 7.6 Hz, 1H), 6.823 ppm (t, J = 8.0 Hz, 1H).

4-(1H-benzo[d]imidazol-2-yl)benzene-1,3-diol: white powder with the yield of 88%. ^{1}H NMR (TMS, DMSO-d6, 400 MHz): δ = 13.202 (s, 1H), 12.930 (s, 1H), 10.011 (s, 1H), 7.849 (d, J = 8.8 Hz, 1H), 7.621 (s, 1H), 7.529 (s, 1H), 7.215 (d, J = 4 Hz, 2H), 6.425 (d, J = 8.4 Hz, 1H), 6.389 ppm (s, 1H).

4-(1H-benzo[d]imidazol-2-yl)benzene-1,2-diol: white powder with the yield of 91%. ^{1}H NMR (TMS, DMSO-d6, 400 MHz): δ = 12.520 (s, 1H), 9.521 (s, 1H), 9.289 (s, 1H), 7.603 (s, 1H), 7.512 (s, 2H), 7.452 (d, J = 8.0 Hz,1H), 7.127-7.146 (m, 2H), 6.862 ppm (d, J = 8.0 Hz, 1H).

General procedure of alkylation reaction: In Ar, the prepared benzimidazole derivatives (0.226 g, 1 mmol), TBAB (0.0644 g, 0.2 mmol), KOH (0.625g, 10 mmol) and 3,6-di-tert-butyl-*N*-(3-chloropropyl)-carbazole (1.007 g, 3 mmol) were dissolved in THF (10 mL) and then heated to 80°C. After stirring for 24 h, the reaction was cooled to room temperature and quenched by addition of water (10 mL). The mixture was extracted by CH_2Cl_2 (3×10 mL). The organic layers were combined and dried with anhydrous Na_2SO_4. Then, the solvent was removed under *vacuo*. The residue was purified by flash column chromatography with a mixture of chloroform and ethyl acetate (40:1, v/v) as the eluent.

*9,9'-(3,3'-(3-(1-(3-(3,6-di-tert-butyl-9H-carbazol-9-yl)propyl)-1H-benzo[d]imidazol-2-yl)-1,2-phenylene)bis(oxy)bis(propane-3,1-diyl))bis(3,6-di-tert-butyl-9H-carbazole) (**23NTCzPBI**)*: white powder with the yield of 33%. ^{1}H NMR (TMS, $CDCl_3$, 400 MHz): δ = 8.129 (s, 2H), 8.082 (s, 2H), 8.059 (s, 2H), 7.890 (d, J = 8.0 Hz, 1H), 7.419 (d, J = 8.8 Hz, 2H), 7.379 (d, J = 8.4 Hz, 2H), 7.186-7.316 (m, 6H), 7.149 (s, 2H), 7.081 (d, J = 8.0 Hz, 1H), 7.036 (d, J = 9.2 Hz, 2H), 7.001 (d, J = 8.4 Hz, 2H), 6.886 (d, J = 8.0 Hz, 1H), 4.398 (t, J = 5.6 Hz, 2H), 4.319 (t, J = 6.8 Hz, 2H), 4.081-4.168 (m, 6H), 4.014 (t, J = 5.2 Hz, 2H) 2.300-2.400 (m, 4H), 1.980-2.081 (m, 2H), 1.457 (s, 18H), 1.429 ppm (s, 36H); MALDI-TOF: m/z (%): 1183 (100) [M^+]; elemental analysis (%) for $C_{82}H_{97}N_5O_2$: C 83.13, H 8.25, N 5.91; found: C 83.15, H 8.24, N 5.94.

*9,9'-(3,3'-(4-(1-(3-(3,6-di-tert-butyl-9H-carbazol-9-yl)propyl)-1H-benzo[d]imidazol-2-yl)-1,3-phenylene)bis(oxy)bis(propane-3,1-diyl))bis(3,6-di-tert-butyl-9H-carbazole) (**24NTCzPBI**)*: white powder with the yield of 41%. ^{1}H NMR (TMS, $CDCl_3$, 400 MHz): δ = 8.147 (d, J = 1.2 Hz, 2H, 8.033 (s, 4H), 7.914 (d, J = 7.2 Hz, 1H), 7.509-7.535 (dd, J_1 = 8.8 Hz, J_2 = 2.0 Hz, 2H), 7.299-7.387 (m, 8H), 7.085-7.111 (dd, J_1 = 8.8 Hz, J_2 = 1.6 Hz, 2H), 6.937 (d, J = 8.8 Hz, 2H), 6.827 (d, J = 8.8 Hz, 2H), 6.468-6.494 (dd, J_1 = 8.4 Hz, J_2 = 2Hz, 1H), 6.282 (d, J = 2 Hz, 1H), 4.555 (t, J = 6.4 Hz, 2H), 4.209 (t, J = 7.6 Hz, 2H), 4.141 (t, J = 7.2 Hz, 2H), 4.123 (t, J = 7.6 Hz, 2H), 4.027 (t, J = 5.6 Hz, 2H), 2.386-2.446 (m, 2H), 2.269-2.339 (m, 2H), 1.952-2.009 (m, 2H), 1.401 (s, 18H), 1.420 ppm (s, 36H); MALDI-TOF: m/z (%): 1183 (100) [M^+]; elemental analysis (%) for $C_{82}H_{97}N_5O_2$: C 83.13, H 8.25, N 5.91; found: C 83.17, H 8.23, N 5.97.

*9,9'-(3,3'-(4-(1-(3-(3,6-di-tert-butyl-9H-carbazol-9-yl)propyl)-1H-benzo[d]imidazol-2-yl)-1,2-phenylene)bis(oxy)bis(propane-3,1-diyl))bis(3,6-di-tert-butyl-9H-carbazole) (**34NTCzPBI**)*: white powder with the yield of 43%. ^{1}H NMR (TMS, $CDCl_3$, 400 MHz): δ = 8.132 (s, 2H), 8.109 (s, 2H), 8.092 (s, 2H), 7.791 (d, J = 7.6Hz, 1H), 7.375-7.467 (m,10H), 7.276 (d, J = 3.6Hz, 2H), 7.169 (t, J = 7.6 Hz, 1H) 7.061 (d, J = 8.8Hz, 2H), 6.979-7.029 (m, 2H), 6.669 (d, J = 8.4Hz, 1H), 4.629 (t, J = 6.0 Hz, 2H), 4.589 (t, J = 6.4 Hz, 2H), 4.181-4.240 (m, 4H), 4.100-4.142 (m, 4H), 2.462-2.540 (m, 2H), 2.386-2.446 (m, 4H), 1.451 (s, 18H), 1.443 (s, 18H), 1.412 ppm (s, 18H); MALDI-TOF: m/z (%): 1183 (100) [M^+]; elemental analysis (%) for $C_{82}H_{97}N_5O_2$: C 83.13, H 8.25, N 5.91; found: C 83.11, H 8.27, N 5.90.

General procedure of complexation: In Ar, ***xyN*TCzPBI** (1.30 g, 1.1 mmol) and $IrCl_3$ nH_2O (n = 1-3, 0.164 g, 0.5 mmol) were dissolved in 2-ethoxyethanol (15 mL), H_2O (15 mL) and THF (5 mL). The mixture was heated to 110 °C and stirred for 24h. Then, the system was cooled to room temperature. The precipitate was collected by filtration and washed with anhydrous ethanol (3×10 mL) to afford the crude chloro-bridged dimer as greenish yellow powder, which was directly used in the next step without further purification. ***xyN*TCzPBI** (0.593 g, 0.5 mmol), dimer (1.3 g, ~0.25

mmol) and K_2CO_3 (0.345 g, 2.5 mmol) were suspended in glycerol (15 mL). The mixture was heated to 240 °C and stirred for 72 h. Then, the system was poured into water (50 mL) and extracted with CH_2Cl_2 (3×50 mL). The organic phase was combined and dried with anhydrous Na_2SO_4. After removal of solvent, the residue was purified by flash column chromatography with petroleum ether and dichloromethane (1:5, v/v) as the eluent.

Ir(23NTCzPBI)$_3$: yellow powder with the total yield of 7%. ^{1}H NMR (TMS, $CDCl_3$, 400 MHz): δ = 8.135 (s, 2H), 8.108 (s, 2H), 8.054-8.062 (m, 6H), 8.021 (s, 8H), 7.281-7.308 (m, 11H), 7.172-7.234 (m, 12H), 7.096-7.134 (m, 6H), 7.033-7.069 (m, 4H), 6.919 (d, J = 8.8Hz, 3H), 6.811 (d, J = 5.6Hz, 2H), 6.835-6.781 (m, 16H), 5.045-5.154 (m, 2H), 4.384-4.604 (m, 6H), 4.123-4.278 (m, 8H), 3.928-4.074 (m, 12H), 3.820-3.843 (m, 2H), 3.664-3.736 (m, 2H), 3.568-3.588 (m, 2H), 3.283-3.339 (m, 2H), 1.870-2.442 (m, 14H), 1.683-1.870 (m, 4H), 1.312-1.408 (m, 162H); ^{13}C NMR ($CDCl_3$, 100 MHz): δ = 168.758, 165.148, 164.776, 152,.444, 152.152, 146.512, 146.354, 145.308, 142.686, 141.865, 141.574, 141.473, 138.894, 138.636, 127.988, 123.99, 123.562, 123.420, 123.143, 122.864, 122.803, 122.739, 122.550, 120.435, 118.292, 117.285, 116.974, 116.536, 115.956, 110.340, 110.103, 108.616, 108.181, 107.978, 72.552, 68.058, 66.413, 53.468, 44.464, 40.370, 40.186, 40.107, 39.810, 34.670, 32.091, 30.969, 29.912, 29.075, 28.039, 27.954 ppm; MALDI-TOF: m/z (%): 3743 (100) [M^+]; elemental analysis (%) for $C_{246}H_{288}IrN_{15}O_6$: C 78.9, H 7.75, N 5.61; found: C 78.7, H 7.76, N 5.69.

Ir(24NTCzPBI)$_3$: yellow powder with the total yield of 13%. ^{1}H NMR (TMS, $CDCl_3$, 400 MHz): δ = 8.051 (s, 6H), 8.022 (s, 6H), 8.000 (s, 6H) , 7.271-7.297 (dd, J_1 = 8.8 Hz, J_2 = 1.6 Hz, 7H) , 7.169-7.195 (dd, J_1 = 8.4 Hz, J_2 = 1.6 Hz, 6H) , 7.080-7.105 (dd, J_1 = 8.4 Hz, J_2 = 1.6 Hz, 7H), 6.997 (t, J = 8.4 Hz, 16H) , 6.873 (t, J = 7.6 Hz, 3H), 6.696 (d, J = 8 Hz, 3H) , 6.537-6.583 (m, 9H), 6.424 (d, J = 1.6 Hz, 3H) , 4.999-5.034 (m, 4H), 4.504-4.567 (m, 4H), 3.538-4.149 (m, 20H), 3.292-3.346 (m, 4H), 3.093-3.146 (m, 4H), 2.331-2.404 (m, 4H), 2.331-2.404 (m, 4H) , 2.004-2.108 (m, 4H), 1.896-1.997 (m, 4H), 1.621-1.653 (m, 2H) , 1.375 (s, 54H) , 1.358 (s, 54H), 1.322 (s, 54H); ^{13}C NMR ($CDCl_3$, 100 MHz): δ = 167.070, 164.552, 161.066,

156.253, 143.063, 141.669, 141.473, 141.342, 138.713, 138.680, 138.554, 135,266, 123.469, 123.233, 123.200, 122.713, 122.619, 118.126, 116.441, 116.317, 116.118, 115.999, 111.053, 108.055, 107.704, 65.668, 64.228, 45.041, 39.925, 39.912, 39.656, 39.558, 34.612, 34.549, 32.086, 32.035, 29.774, 28.692, 28.446, 27.716 ppm; MALDI-TOF: m/z (%): 3743 (100) [M^+]; elemental analysis (%) for $C_{246}H_{288}IrN_{15}O_6$: C 78.9, H 7.75, N 5.61; found: C 78.5, H 7.77, N 5.65.

Ir(34NTCzPBI)$_3$: yellow powder with the total yield of 13%. ^{1}H NMR (TMS, $CDCl_3$, 400 MHz): δ = 8.050 (s, 6H), 8.027 (s, 12H) , 7.214-7.316 (m, 27H), 7.139 (d, J = 8.8 Hz, 6H), 6.867 (d, J = 8.4 Hz, 6H), 6.886 (t, J = 7.6 Hz, 3H), 6.691 (d, J = 8.4 Hz, 3H) , 6.546-6.592 (m, 6H), 6.128 (d, J = 8 Hz, 3H) , 4.360-4.520 (m, 6H) , 4.200-4.360 (m, 12H), 4.000-4.100 (m, 6H) , 3.820-3.920 (m, 12H), 2.280-2.320 (m, 6H), 2.180-2.260 (m, 6H), 1.960-2.100 (m, 6H), 1.357 (s, 54H) , 1.331 (s, 54H) , 1.304 (s, 54H); ^{13}C NMR ($CDCl_3$, 100 MHz): δ = 162.042, 162.024, 159.415, 150.943, 150.924, 142.298, 142.038, 141.601, 139.100, 138.839, 138.594, 135.119, 126.904, 123.594, 123.432, 122.927, 122.838, 122.775, 121.572, 121.521, 121.464, 116.407, 116.335, 116.234, 113.399, 108.996, 108.064, 107.992, 107.770, 82.798, 67.903, 65.252, 42.149, 42.125, 40.228, 40.104, 40.083, 40.045, 40.023, 34.630, 34.604, 32.043, 30.955, 29.606, 28.928, 28.733 ppm; MALDI-TOF: m/z (%): 3743 (100) [M^+]; elemental analysis (%) for $C_{246}H_{288}IrN_{15}O_6$: C 78.9, H 7.75, N 5.61; found: C 79.0, H 7.71, N 5.66.

DFT Calculations

DFT computations were carried out with different parameters for structure optimizations and vibration analyses. The ground states of molecules in *vacuum* were optimized without any assistance of experimental data by the restricted and unrestricted formalism of Beck's three-parameter hybrid exchange functional[1] and Lee, and Yang and Parr correlation functional[2] (B3LYP) for C, H, N, and O and effective core potential (ECP) of LANL2DZ for Ir. The optimization was performed at the level of 6-31G(d). The fully optimized stationary points were further characterized by harmonic vibrational frequency analysis to ensure that real local minima had been found without imaginary vibrational frequency. The total energies were also corrected

by zero-point energy both for the ground state. All computations were performed using the Gaussian 03 package.[3]

Device Fabrication and Testing

TPBi is 1,3,5-tris(1-phenyl-1H-benzo[d]imidazol-2-yl)benzene as electron transporting and hole blocking layer, and TCTA is tris(4-(9H-carbazol-9-yl)phenyl)amine as host, respectively. Before loading into a deposition chamber, the ITO substrate was cleaned with detergents and deionized water, dried in an oven at 120 °C for 4 h, and treated with UV-ozone for 20 min. Devices were fabricated by evaporating organic layers at a rate of 0.1-0.3 nm s^{-1} onto the ITO substrate sequentially at a pressure below 1×10^{-6} mbar. Onto the TPBI layer, a layer of LiF with 0.5 nm thickness was deposited at a rate of 0.1 nm s^{-1} to improve electron injection. Finally, a 100-nm-thick layer of Al was deposited at a rate of 0.6 nm s^{-1} as the cathode. The emission area of the devices was 0.14 cm^2 as determined by the overlap area of the anode and the cathode. The EL spectra and CIE coordinates were measured using a PR650 spectra colorimeter. The current-density-voltage and brightness–voltage curves of the devices were measured using a Keithley 2400/2000 source meter and a calibrated silicon photodiode. All the experiments and measurements were carried out at room temperature under ambient conditions.

AFM Image of Ir(*xyN*TCzPBI)$_3$-based Neat and Doped Films

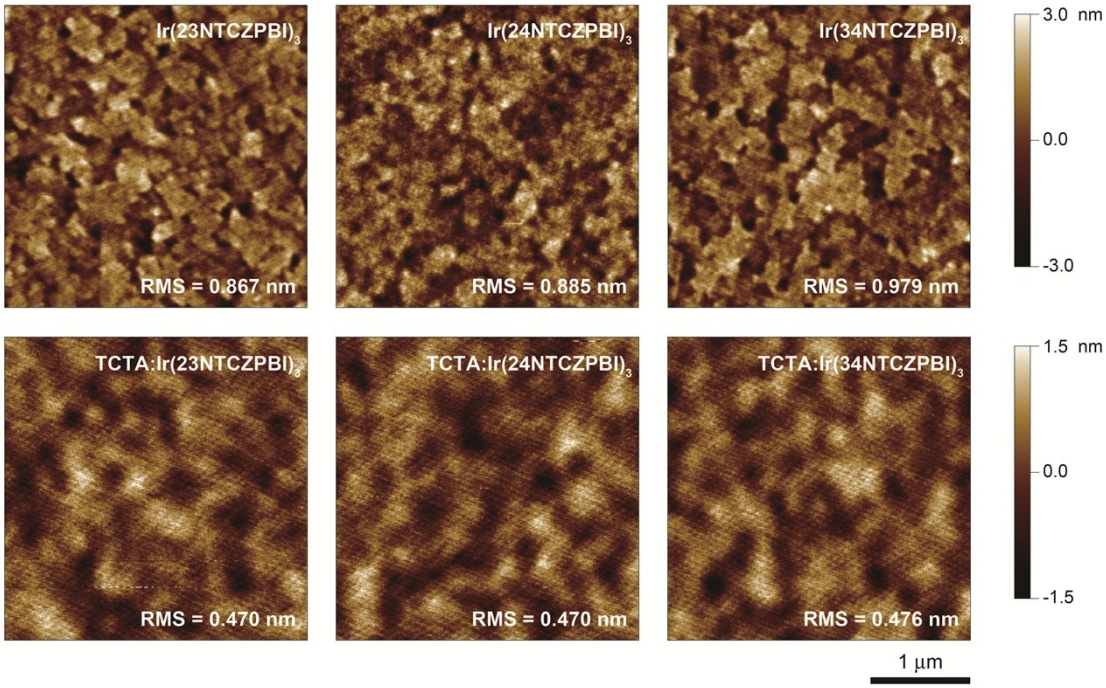

Figure S1. AFM images of neat **Ir(*xyN*TCzPBI)$_3$** films and codoped films in TCTA (20%wt) with the thickness of 100 nm.

The AFM images of neat **Ir(*xyN*TCzPBI)$_3$** films with thickness of 100 nm showed the uniformly distributed nanoscale patterns, which should be attributed to the ordered stacking of these nanosize complexes rather than aggregation or crystallization. Furthermore, from **Ir(*23N*TCzPBI)$_3$**, **Ir(*24N*TCzPBI)$_3$** to **Ir(*34N*TCzPBI)$_3$**, the root mean square (RMS) roughness of their neat films was gradually increased from 0.867, 0.885 to 0.979 nm, respectively, in accord with the molecular volumes of these complexes. After doped in TCTA, all of the films revealed the equivalent and halved RMS roughness around 0.47 nm.

Thermal Properties of Ir(*xyN*TCzPBI)$_3$

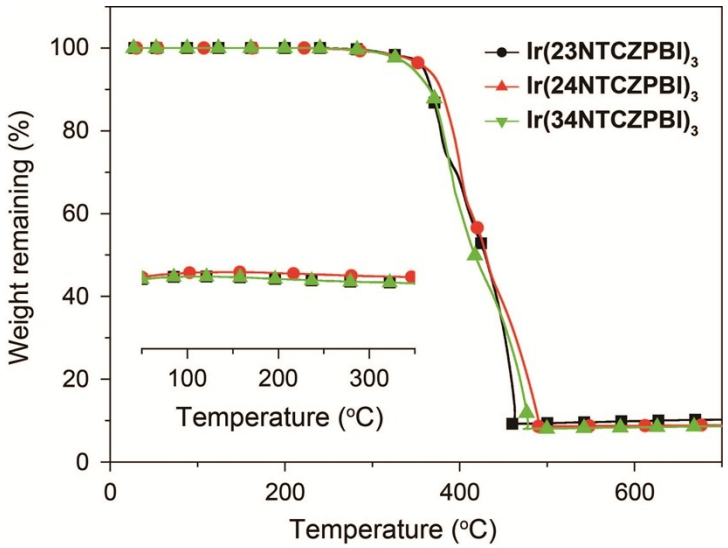

Figure S2. TGA and DSC (inset) curves of **Ir(*xyN*TCzPBI)$_3$**.

Transient Emission Properties of Ir(*xyN*TCzPBI)$_3$ in Solution

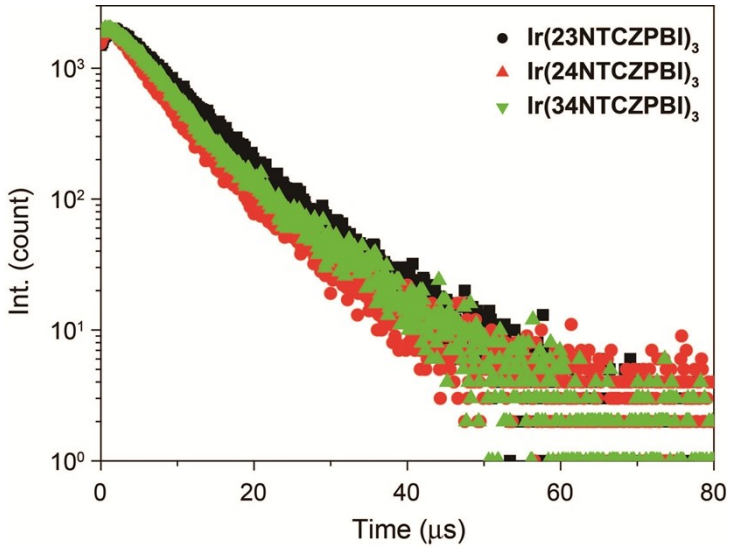

Figure S3. Time decay curves of **Ir(*xyN*TCzPBI)$_3$** in degassed CH_2Cl_2 (10^{-6} mol L^{-1}) at room temperature.

Solid-State Emission Properties of Ir(*xyN*TCzPBI)$_3$

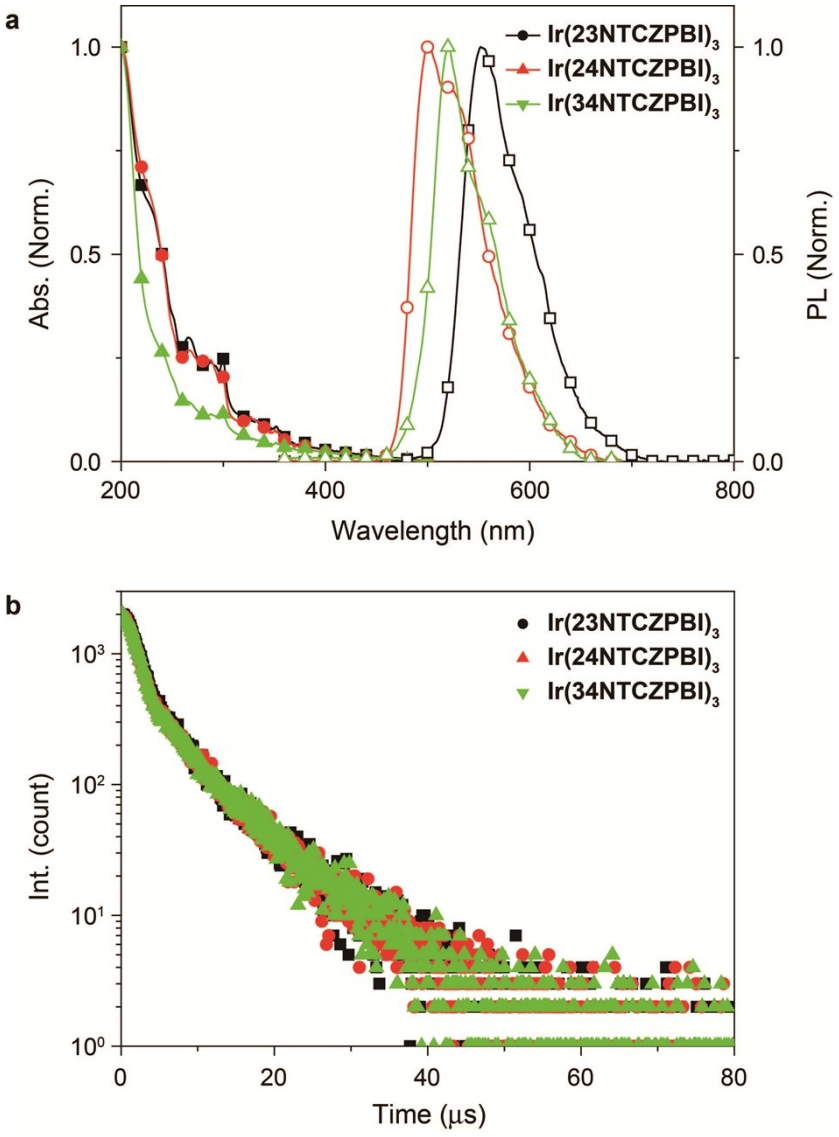

Figure S4. a. UV/vis absorption (abs.) and photoluminescence (PL) spectra of spin-coated films for **Ir(*xyN*TCzPBI)$_3$**; **b.** Time decay curves of **Ir(*xyN*TCzPBI)$_3$** in films.

Device Structure of the Nondoped Devices

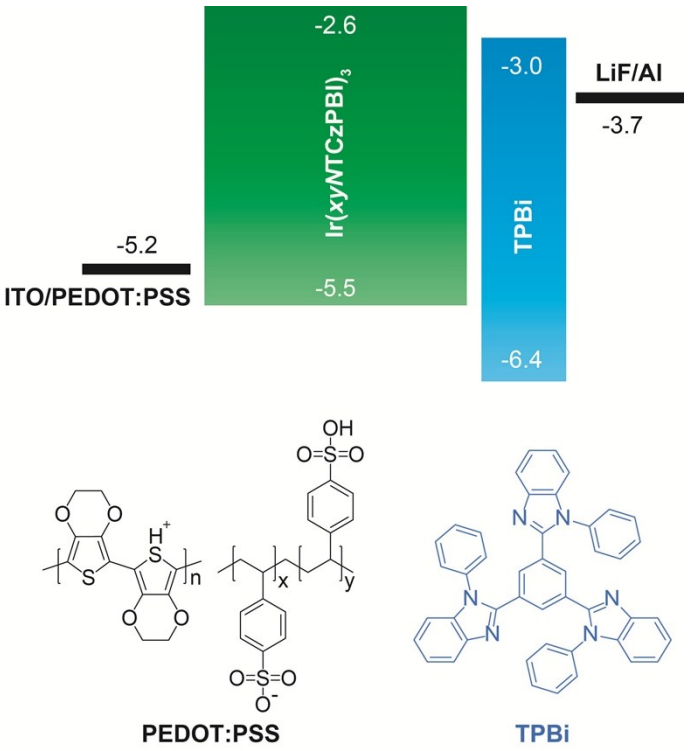

Scheme S2. Device configuration and energy level scheme of the host-free devices and the chemical structures of the involved materials.

EL Performance of Doped Devices

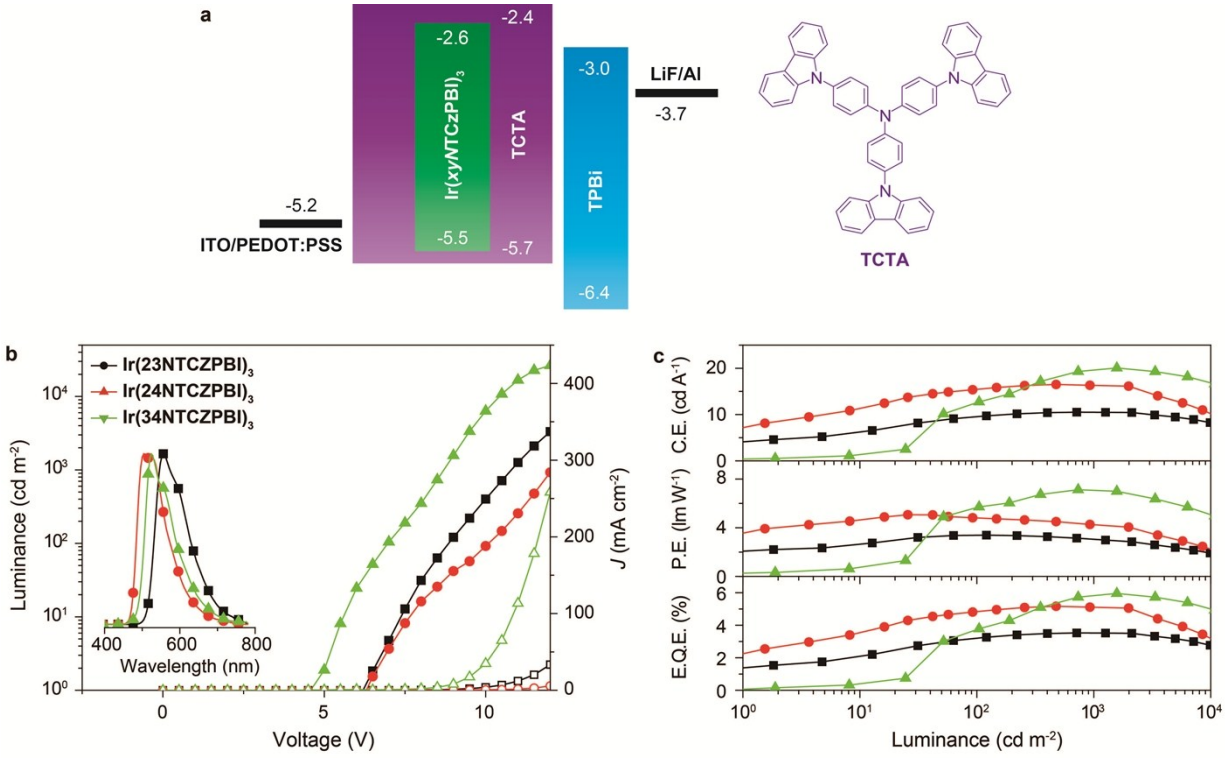

Figure S5. a. Device configuration of **Ir(*xyN*TCzPBI)$_3$**-doped bilayer spin-coated OLEDs as ITO|PEDOT:PSS (50nm)|TCTA:**Ir(*xyN*TCzPBI)$_3$** (10%wt., 40nm)|TPBi (30nm)|LiF (1nm)|Al and energy level scheme; **b.** Luminance-current density (*J*)-voltage curves and EL spectra (inset) of; **c.** Efficiency-luminance curves of the devices.

Table S1 Physical properties of Ir(*xyN*TCzPBI)$_3$.

Phosphor	Absorption (nm)	Phosphorescence (nm)	PLQY[c] (%)	Lifetime (μs)	T_1[d] (eV)	T_d (^{o}C)	HOMO[e] (eV)	LUMO[e] (eV)
Ir(*23N*TCzPBI)$_3$	351,320,290,260,240[a]	563[a]	52[a]	7.75[a]	2.28	358	-5.35	-2.69
	351,300,288,266,232[b]	552,591[b]	35[b]	6.13[b]				
Ir(*24N*TCzPBI)$_3$	351,325,290,260,240 [a]	505,529[a]	75[a]	6.49[a]	2.53	362	-5.49	-2.34
	351,300,288,266,232[b]	500,518[b]	64[b]	6.12[b]				
Ir(*34N*TCzPBI)$_3$	351,320,290,260,240[a]	523,554[a]	73[a]	6.52[a]	2.44	346	-5.42	-2.41
	351,300,288,266, 238[b]	520,551[b]	72[b]	6.19[b]				

[a] In CH_2Cl_2 (10^{-6} mol L^{-1}); [b] in film; [c] measured with integrating sphere; [d] estimated according to the 0-0 transition of low-temperature emission spectra; [e] calculated according the onset voltages of redox peaks with the equation of -(V_{onset} + 4.78) eV.

Table S2 EL performance of Ir(*xyN*TCzPBI)$_3$-based OLEDs.

Emitter	Operating Voltage (V)[a]	Maximum Efficiencies[b]	Efficiency Roll-Offs (%)[c]		
			CE	PE	EQE
Nondoped devices					
Ir(*23N*TCzPBI)$_3$	5.5, <8.0, <10.0	5.15, 1.7, 1.8	-, -	-, 5.9	-, -
Ir(*24N*TCzPBI)$_3$	5.0, <8.0, <10.0	16.7, 9.2, 5.6	1.2, 30.5	26, 60.8	0.9, 30.2
Ir(*34N*TCzPBI)$_3$	3.5, <5.0, <6.0	27.7, 15.4, 8.3	-, 0.4	-, 8.4	-, 0.5
Doped devices					
Ir(*23N*TCzPBI)$_3$	6.5, <9.0, <11.0	10.5, 3.4, 3.5	-, 0.3	-, 11.8	-, 0.3
Ir(*24N*TCzPBI)$_3$	6.5, <10.5, <12.5	16.5, 5.0, 5.2	-, 0.8	3.6, 14.6	-, 1.9
Ir(*34N*TCzPBI)$_3$	5.0, <7.0, <9.0	20.0, 7.1, 5.9	-, -	-, 1.5	-, -

[a] In the order of onset, 100 and 1000 cd m^{-2}; [b] in the order of CE (cd A^{-1}), PE (lm W^{-1}) and EQE (%); [c] in the order of 100 and 1000 cd m^{-2}.

References

1 A. D. Becke, *J. Chem. Phys.*, 1993, **98**, 5648.

2 C. Lee, W. Yang and R. G. Parr, *Phys. Rev. B*, 1988, **37**, 785.

3 M. J. Frisch, G. W. Trucks, H. B. Schlegel, G. E. Scuseria, M. A. Robb, J. R. Cheeseman, J. A. Montgomery, J. T. Vreyen, K. N. Kudin, J. C. Burant, J. M. Millam, S. S. Iyengar, J. Tomasi, V. Barone, B. Mennucci, M. Cossi, G. Scalmani, N. Rega, G. A. Petersson, H. Nakatsuji, M. Hada, M. Ehara, K. Toyota, R. Fukuda, J. Hasegawa, M. Ishida, T. Nakajima, Y. Honda, O. Kitao, H. Nakai, M. Klene, X. Li, J. E. Knox, H. P. Hratchian, J. B. Cross, C. Adamo, J. Jaramillo, R. Gomperts, R. E. Stratmann, O. Yazyev, A. J. Austin, R. Cammi, C. Pomelli, J. W. Octhterski, P. Y. Ayala, K. Morokuma, G. A. Voth, P. Salvador, J. J. Dannenberg, V. G. Zakrzewski, S. Dapprich, A. D. Daniels, M. C. Strain, O. Farkas, D. K. Malick, A. D. Rabuck, K. Raghavachari, J. B. Foresman, J. V. Ortiz, Q. Cui, A. G. Baboul, S. Clifford, J. Cioslowski, B. B. Stefanov, A. L. G. Liu, P. Piskorz, I. Komaromi, R. L.Martin, D. J. Fox, T. Keith, M. A. Al-Laham, C. Y. Peng, A. Nanayakkara, M. Challacombe, P. M. W. Gill, B. Johnson, W. Chen, M. W. Wong, C. Gonzalez and J. A. Pople, *Gaussian 03, Revision D.02, Gaussian Inc., Pittsburgh, PA*, 2004.